Research Article

Ebrahem A. Algehyne, Humaira Yasmin*, Fahad Maqbul Alamrani, Fuad S. Alduais, and Afrah Al-Bossly

Impact of nanoparticle shapes on the heat transfer properties of Cu and CuO nanofluids flowing over a stretching surface with slip effects: A computational study

https://doi.org/10.1515/phys-2025-0184
received February 23, 2025; accepted May 12, 2025

Abstract: This study investigates thermally radiative nanofluid flows on an elongating surface using porous media. The flow dynamics are affected by the combined impacts of exponential and thermally dependent heat sources. Additionally, magnetic effects are introduced to the flow system while it is inclined. Copper (Cu) and copper oxide (CuO) nanoparticles are mixed in water (H_2O) to fabricate nanofluid flows. Different shapes of Cu and CuO nanoparticles, including column, sphere, hexahedron, tetrahedron, and lamina, were studied in this analysis. The system flow is triggered by the stretching properties of the sheet. The textured surface of the stretching sheet facilitates the exploration of the slip velocity phenomenon. The modeled equations are evaluated using the bvp4c approach in a dimensionless form. The present study is validated by comparing its findings with established datasets available in the literature. The results of this analysis show that the velocity distributions decline with increasing values of the porosity factor, velocity slip factor, and magnetic factor. The reduction in velocity profiles is quite significant in the case of Cu–water nanofluid, in contrast to the CuO–water nanofluid due to more dominance of resistive constraints in the case of the Cu–water nanofluid. The thermal distribution increases with an increase in the magnetic factor, radiation factor, Eckert number, thermal-dependent heat source, and space-based heat source, and declines with an increase in the inclination angle and thermal slip factor. The Nusselt number augments for both types of nanofluids with an increase in various emerging factors in the scenarios of thermal slip and no-slip, where an increase in the Nusselt number is maximum for the scenario where there is no thermal slip. A higher thermal distribution and heat transfer rate are determined for the lamina-shaped Cu–water and CuO–water nanofluid flows for both slip and no-slip thermal conditions. On the basis of the current findings, this study aims to design efficient cooling systems for microelectronics, improve solar thermal collectors, enhance drug delivery *via* heat-sensitive nanoparticles, optimize industrial heat exchangers, and advance smart textile technologies requiring controlled thermal regulation using shape-engineered Cu and CuO nanofluids.

Keywords: nanofluid, inclined magnetic field, porous media, heat source, slip conditions, Joule heating, numerical investigation

*** Corresponding author: Humaira Yasmin,** Department of Basic Sciences, General Administration of Preparatory Year, King Faisal University, P.O. Box 400, Al Ahsa, 31982, Saudi Arabia; Department of Mathematics and Statistics, College of Science, King Faisal University, P.O. Box 400, Al Ahsa, 31982, Saudi Arabia, e-mail: hhassain@kfu.edu.sa
Ebrahem A. Algehyne, Fahad Maqbul Alamrani: Department of Mathematics, Faculty of Science, University of Tabuk, P.O. Box 741, Tabuk, 71491, Saudi Arabia
Fuad S. Alduais, Afrah Al-Bossly: Department of Mathematics, College of Science and Humanities in Al-Kharj, Prince Sattam bin Abdulaziz University, Al-Kharj, 11942, Saudi Arabia

Nomenclature

u, v	flow components [m s^{-1}]
b	stretching constant
$u_w(x)$	stretching velocity [m s^{-1}]
B_0	strength of the magnetic field [kg s^{-2} A^{-1}]
T	temperature [K]
k^*	mean absorption coefficient [m^{-1}]
C_p	specific heat [J kg^{-1} K^{-1}]
Q_t	thermal-dependent heat source coefficient [W m^{-3} K^{-1}]
Q_e	space-dependent heat source coefficient [W m^{-3} K^{-1}]
k	thermal conductivity [W K^{-1} m^{-1}]

n	power index
ν	kinematic viscosity [$m^2\ s^{-1}$]
$f(\eta)$	velocity profile
M	magnetic factor
K	porosity parameter
Rd	thermal radiation factor
Ec	Eckert number
Q_{Exp}	exponential heat source
Q_I	thermal-dependent heat source

Greek notation

ρ	density [$kg\ m^{-3}$]
σ	electrical conductivity [$S\ m^{-1}$]
$\theta(\eta)$	temperature profile
φ	volume fraction of the nanoparticle
σ_1	coefficient of velocity slip
σ_2	coefficient of thermal slip
η	variable
γ	acute angle [$()^0$]
μ	dynamic viscosity [$kg\ m^{-1}\ s^{-1}$]
λ_1	velocity slip factor
λ_2	thermal radiation factor

Subscripts

∞	free-stream
N	nanoparticle
f	fluid
nf	nanofluid

1 Introduction

Nanofluids are composed of a combination of nanoparticles and pure fluid, where both are mixed. The accumulation of nanoparticles alters the thermal, optical, and rheological features of the base fluid, resulting in nanofluids with enhanced heat transfer capabilities associated with conventional fluids, as observed by Choi and Eastman [1]. This enhancement arises primarily from the high surface area-to-volume ratio and unique thermal conductivities of the nanoparticles [2]. Acharya *et al.* [3] have proved that a nanolayer greatly impacts the heat transference in comparison to the nanoparticles' diameter. The Brownian motion of nanoparticles within the fluid helps distribute heat more effectively, while the increased thermal conductivity enables faster and more efficient heat transfer [4]. Achieving stable dispersion and preventing particle agglomeration are critical challenges in nanofluid synthesis and application and are often addressed through surface modification, surfactants, or stabilizers. The applications of these fluids are there are industries, comprising heat exchangers, solar energy systems, automotive cooling, and biomedical devices, owing to their superior heat transfer performance and potential for tailored properties [5,6]. Ongoing research continues to explore new nanofluid formulations, synthesis methods, and applications to further optimize their properties and expand their utility in diverse engineering and scientific domains. With the passage of time, the dispersion of two or more distinct nanoparticles can further heighten the thermal flow behavior of a pure fluid, also termed a hybrid nanofluid [7]. Hybrid nanofluid flow represents an innovative area of research in thermal engineering, where the introduction of several kinds of nanoparticles into a pure fluid creates a composite fluid with enhanced heat transfer properties [8]. This innovative approach capitalizes on the synergistic effects of combining different nanoparticle materials, such as metallic and non-metallic particles, to tailor the fluid's thermal conductivity, viscosity, and other key characteristics for specific applications [9,10]. The occurrence of nanoparticles in pure fluid leads to effective heat dissipation and has led to the development of coolants and heat exchangers for thermal performance systems [11]. Additionally, the hybrid nature of these nanofluids allows for the optimization of other heat transfer-related properties, such as convective heat transfer coefficients. Furthermore, the unique rheological behavior of hybrid nanofluids can alter flow patterns and heat transfer mechanisms, presenting opportunities for enhancing heat transfer rates and optimizing system design [12]. Upreti *et al.* [13] used the heterogeneous as well as homogeneous reactions for nanofluid flow on an elongated sheet with the famous Buongiorno model and convective constraints. Adnan *et al.* [14] simulated numerically the thermal features for nanofluid flow using dissipative effects and convective heat constraints influences, and noticed that thermal flow is affected less by the slippery features of the surface, while growth in dissipative factor has augmented thermal profiles to the maximum level. Rahman *et al.* [15] studied the thermally Darcy–Forchheimer fluid flow on a medium with impressions of a magnetic field and heating source. Alharbi *et al.* [16] investigated the thermal management for nanofluid flow through the annular region affected by radiative and magnetized processes. Bani-Fawaz *et al.* [17] studied the thermal flow phenomenon for radiated nanoparticle flow influenced by the diameter of molecules

and the features of nanoparticles. Rawat *et al.* [18] used non-Fick and non-Fourier phenomena to investigate mixed convective magneto-hydrodynamic (MHD) fluid flows. Upreti *et al.* [19] assessed the thermally blood-based nanofluid flow on a permeable surface with impressions of a magnetic field and the Cattneo–Christov model and have observed dual features in flow profiles for augmentation in the magnetic factor. Upreti *et al.* [20] assessed convective thermal flow for Sisko fluid flow on a stretchable surface with suction and dissipative effects. Gangadhar *et al.* [21] discussed Stefan blowing effects on fluid flow past a spinning convective disk with effects of chemical reactivity. Ahmed *et al.* [22] investigated the peristaltic propulsion of thermal radiative magnetized nanofluid flow incorporating the lubrication approximation and slip boundary conditions. Their study focused on understanding how thermal radiation and magnetic fields influence the movement and heat transfer behavior of nanoparticles in a peristaltic transport system. Hayat *et al.* [23] studied the peristaltic hybrid nanoparticle flow through a channel with the impacts of heated asymmetric configurations. Gangadhar *et al.* [24] explored the nonlinear radiative heat transfer in a nanofluid flow over a permeable inclined surface, considering the effects of chemical reactivity. Their study focused on understanding the influence of radiative heat and chemical reactions on the thermal and flow characteristics of nanofluids under various conditions.

An inclined magnetic field is a magnetic field whose direction varies from horizontal or vertical. In such scenarios, the Lorentz force, generated from the interaction between the conducted (electrically) fluid and magnetic field, becomes a dominant factor in determining the flow dynamics [25,26]. This force exerts a deflecting influence on the fluid flow, causing deviations in the velocity profiles and shear stresses within the fluid. These changes, in turn, profoundly affect the mechanisms of convective heat transfer [27]. Forced convection, driven by external forces or pressure gradients, experiences modifications due to Lorentz force-induced alterations in the flow direction and velocity distribution. Similarly, natural convection, driven by buoyancy forces resulting from temperature gradients, undergoes significant transformations with the effect of an inclined magnetic field [28]. The Lorentz force-induced modifications in the flow dynamics disrupt the buoyancy-driven flow patterns, causing changes in the heat transfer rates and temperature distributions within the fluid. The composite phenomenon amid fluid flow, magnetic fields, and heat transfer in inclined magnetic field configurations is crucial for numerous engineering applications, such as system coolants [29,30]. Additionally, such an understanding is relevant in various natural phenomena and industrial processes, such as geophysical fluid dynamics, metallurgical processes, and the operation of MHD systems in fusion reactors and space propulsion technologies. Saeed *et al.* [31] examined convective slip fluid flow with double diffusive behavior for nanofluid on an asymmetric conduit. Gangadhar *et al.* [32] examined the entropy optimization and impacts of electro-magneto-hydrodynamics on nanofluid flow with nonlinear thermal radiations on a surface. Lone *et al.* [33] examined thermally MHD nanofluid flow through elongating angular spinning disks with varying porosity and the Cattaneo–Christov thermal flux model. Gangadhar *et al.* [34] studied Williamson fluid flow on a Riga surface with effects of nonlinear radiative flux and binary chemically reactive effects. Mahabaleshwar *et al.* [35] studied injection and radiation effects on Newtonian fluid flow on a permeable shrinking surface with the Brinkman model. Gangadhar *et al.* [36] examined computationally the heterogeneous-homogeneous chemically reactive effects on Maxwell fluid flow on a disk with effects of nonlinear thermal radiations. Mahabaleshwar *et al.* [37] investigated the exact solution of fluid flow over a permeable surface, considering different boundary constraints. Their study focused on analyzing how these constraints affect flow behavior, providing valuable insights into fluid dynamics. Their research enhances the understanding of boundary layer theory in engineering and scientific applications.

Porous media are materials with interrelated void spaces or pores that allow the passage or flow of fluids through them. The structure and properties of porous media play vital roles in various engineering and scientific fields. Fluid flow through porous media and its impacts on heat transfer processes are critical phenomena with wide-ranging implications in various engineering and scientific fields [38]. Whenever a liquid flows on a permeable medium, such as soil, sand, or a porous structure, it interacts with the solid matrix and undergoes complex flow behaviors. The porous spaces familiarize resistance to the flow, altering velocity profiles and flow patterns in a way that describes how it impacts heat transfer mechanisms [39]. The interaction between thermal transference and liquid flow on permeable media influences important processes like groundwater flow and thermal energy storage in geothermal reservoirs [40], as well as industrial applications like enhanced oil recovery, geotechnical engineering, and the design of heat exchangers and porous materials for thermal insulation [41]. These phenomena require advanced mathematical models, experimental techniques, and computational simulations to characterize the complex fluid–solid interactions and optimize the processes for efficient energy utilization and sustainable engineering practices. Habibishandiz and Saghir [42] reviewed

critically the augmentation of thermal transmission for nanofluid flow on porous media using the effects of microorganisms. Verma *et al.* [43] examined fluid flow on a penetrable surface using double stratification with the surface as a nonlinearly elongating sheet.

A thermal and space-dependent heat source is a source of thermal energy that varies in both intensity and spatial distribution over time. Thermal- and space-dependent heat sources represent a complex scenario in which both the intensity and spatial distribution of heat generation vary over time. Such heat sources are encountered in numerous engineering and scientific contexts, ranging from industrial processes to environmental systems [44,45]. One common example is found in electronic devices, where the power dissipation within the device fluctuates due to varying operational conditions and computational demands. In this case, the heat generation not only changes over time but also exhibits spatial variations within the device, with certain regions experiencing higher heat fluxes than others [46]. Another example can be seen in combustion systems, where fuel combustion rates may vary due to changes in operating conditions or fuel composition, leading to fluctuations in heat release rates and spatial distributions of heat within the combustion chamber. The impacts of thermal- and space-dependent heat sources on the heat transfer processes are insightful [47]. They affect the temperature distributions, velocity profiles, and flow patterns within the surrounding medium, leading to variations in the convective heat transfer rates [48]. Additionally, these fluctuations can influence the thermal stresses, material degradation, and system performance. Accurately modeling the behavior of thermal and space-dependent heat sources is essential for optimizing heat transfer systems, designing effective cooling strategies, and ensuring the reliability and efficiency of various engineering systems, including electronic cooling systems, thermal management in buildings, and combustion processes in power generation and propulsion systems. Various theoretical analyses have been conducted to characterize the interactions between these heat sources and their surrounding environments, smoothing the progress of innovative solutions in many practical applications [49,50].

The slip conditions illustrate the performance of a fluid flow at a solid boundary, where the fluid molecules interact differently with the surface compared to the bulk fluid. The slip conditions deviate from this assumption, allowing for nonzero velocities at the borderline. Slip conditions are particularly relevant in microfluidics, nanofluidics, and other situations involving fluid flow at small length scales, where intermolecular forces become significant. Fluid flow with slip conditions, where the velocity at the solid boundary differs from that of the bulk fluid, has profound implications for thermal transport processes [51,52]. In such scenarios, the slip alters the velocity profile near the boundary, thereby influencing the thermal transfer rate and temperature distribution within the fluid [53]. At the micro- and nanoscales, where slip effects become increasingly significant, understanding the relationship between fluid flow, slip conditions, and thermal transport is crucial for various applications. For instance, in microfluidic heat exchangers, slip-induced changes in flow behavior can impact the heat transfer efficiency and overall device performance. Similarly, in nanoscale thermal management systems, such as heat dissipation in electronic devices, slip conditions may affect the temperature gradients and heat transfer rates, thereby influencing device reliability and performance [54]. Nazeer *et al.* [55] inspected Hall current and slip constraints at the boundaries for nanofluid flow in a convergent conduit. Amer *et al.* [56] studied the slip effects of fluid flow on an extending sheet with permeable impressions and revealed that slip flow constraints significantly affect the flow phenomenon of the system. Rasool *et al.* [57] inspected the nanofluid unsteady flow with the impact of slip conditions. Lone *et al.* [58] investigated MHD blood-based nanofluid flow over a convectively heated sheet, considering variable porosity and slip conditions at the surface. Their study focused on analyzing how magnetic fields and surface constraints affect heat transfer and flow behavior in biomedical and engineering applications involving nanofluids.

1.1 Novelty

This study thermally investigates radiative nanofluids flowing on an elongating sheet using a permeable sheet. The flow dynamics are affected by the combined impacts of exponential and thermal-dependent heat sources. Additionally, magnetic effects have been introduced to the flow system while it is inclined. Copper (Cu) and copper oxide (CuO) nanoparticles were mixed with water (H_2O) to fabricate nanofluid flows. In this analysis, we focused on the different shapes of the Cu and CuO nanoparticles, which include column, sphere, hexahedron, tetrahedron, and lamina, to explore the thermal panels and their transmission rate. Furthermore, velocity and thermal slip conditions are executed in this analysis to investigate the nanofluid flows. The Joule heating, space-dependent heat source, and thermal-dependent heat source effects are also used in this analysis. Based on these assumptions, we focused on the following research questions:

- What are the impressions of the porosity factor and velocity slip factor on the velocity distributions of the Cu–water and CuO–water nanofluids?

- How do the velocity panels change in response to enhancing the inclination angle with respect to the magnetic field effect, and at what angles are the velocities maximized?
- How do the thermal distribution and Nusselt number change for distinct types of nanofluids under various emerging factors, especially when comparing the thermal slip and no-slip conditions, and where is the maximum increase observed?
- What differences are observed in the thermal distribution and heat transfer rate for lamina-shaped Cu–water and CuO–water nanofluid under slip and no-slip thermal conditions?

The choice of differently shaped nanoparticles is based on their representative nature in real-world applications and their distinctive effects on thermal conductivity, flow behavior, and nanofluid performance. Spherical nanoparticles are often used in experimental studies due to their ease of fabrication and well-documented behavior in terms of flow and heat transfer properties. Column-shaped nanoparticles are relevant for applications where extended structures interact with the fluid, such as nano coatings or heat exchangers, where the elongated shape can enhance the temperature performance. Hexahedral and tetrahedral-shaped nanoparticles have been investigated in the literature due to their geometrical advantages in terms of maximizing the surface area contact with the base fluid, which can impact the heat transfer characteristics. Lamina-shaped nanoparticles are considered due to their potential application in high thermal conductivity systems, where structures can form layered flow paths in nanofluids.

1.2 Practical applications of the problem

Research on the impact of nanoparticle shapes on the heat transfer properties of Cu and CuO nanofluids has a wide range of practical applications. In industrial cooling systems, it can optimize the performance of heat exchangers, thereby improving the efficiency of the cooling processes in power plants, air conditioning, and refrigeration systems. For microelectronics, understanding how different nanoparticle shapes affect heat transfer is vital for thermal management in advanced devices like microchips and computer processors, which require efficient cooling to prevent overheating and enhance performance. In the biomedical field, this study has potential applications in drug delivery systems, where nanofluids can be designed to improve the controlled release of medication by manipulating heat transfer at the targeted site. Furthermore, this research can enhance the efficiency of solar thermal collectors by utilizing nanofluids with optimized nanoparticle shapes to improve heat absorption and transfer, contributing to more effective renewable energy storage systems.

2 Problem formulation

Take an unsteady, laminar, and incompressible flow of nanofluids on a permeable extending surface. A two-dimensional Cartesian coordinate system is chosen for the fluid flows. The sheet expands with velocity $u_w(x) = bx$ along the x-axis, where $b(>0)$ is constant. A magnetic field with strength B_0 acts in an inclined direction with an angle γ in the y-direction, which acts as a transverse magnetic field when $\gamma = 90^\circ$, as shown in Figure 1. Velocity and temperature slip conditions were imposed to inspect the nanofluid flows and heat transfer rate. The surface and ambient temperatures are T_w and T_∞, respectively. Joule heating, space-dependent heat source, thermal-dependent heat source, and thermal radiation impacts are also considered in this study.

Using these assumptions, we have [59]

Continuity equation:

$$u_x + v_y = 0. \tag{1}$$

Momentum equation:

$$\rho_{\mathrm{nf}}(uu_x + vu_y) = \mu_{\mathrm{nf}}u_{yy} - \mu_{\mathrm{nf}}\frac{u}{K_{\mathrm{p}}} - \sigma_{\mathrm{nf}}B_0^2 u\sin^2\gamma. \tag{2}$$

Energy equation:

$$\begin{aligned}(\rho C_{\mathrm{p}})_{\mathrm{nf}}(uT_x + vT_y) &= \left(k_{\mathrm{nf}} + \frac{16\sigma^* T_\infty^3}{3k^*}\right)T_{yy} + \sigma_{\mathrm{nf}}B_0^2u^2\sin^2\gamma \\ &\quad + Q_t(T - T_\infty) + (T_w - T_\infty)Q_e e^{\left(-n\sqrt{\frac{b}{\nu_{\mathrm{f}}}}y\right)}.\end{aligned} \tag{3}$$

The conditions at the boundary are

$$\left.\begin{aligned}&u = u_w(x) + \sigma_1\frac{\partial u}{\partial y}, \quad v = 0, \quad T = T_w + \sigma_2\frac{\partial T}{\partial y}, \\ &\text{at} \quad y = 0, \\ &u \to 0, \quad T \to T_\infty \quad \text{as} \quad y \to \infty.\end{aligned}\right\} \tag{4}$$

The effective qualities of nanofluids are defined as [60–62]:

$$\mu_{\mathrm{nf}} = \frac{\mu_{\mathrm{f}}}{(1-\varphi)^{2.5}}, \tag{5}$$

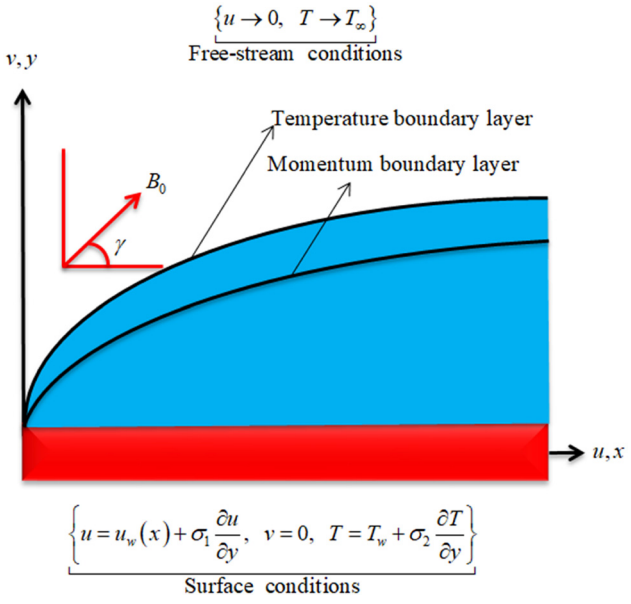

Figure 1: Graphical view of the flow phenomenon.

$$\rho_{nf} = \rho_f(1-\varphi) + \rho_N\varphi, \tag{6}$$

$$(\rho C_p)_{nf} = (1-\varphi)(\rho C_p)_f + \varphi(\rho C_p)_N, \tag{7}$$

$$\frac{k_{nf}}{k_f} = \frac{k_N + (m-1)k_f - (m-1)\varphi(k_f - k_N)}{k_N + (m-1)k_f + \varphi(k_f - k_N)}, \tag{8}$$

$$\frac{\sigma_{nf}}{\sigma_f} = 1 + \frac{3\left(\frac{\sigma_N}{\sigma_f} - 1\right)\varphi - 2(\sigma_f - \sigma_N) + 2\sigma_f}{\left(\frac{\sigma_N}{\sigma_f} + 2\right) - \left(\frac{\sigma_N}{\sigma_f} - 1\right)\varphi}. \tag{9}$$

Here, N represents the nanoparticle, φ is the nanoparticles' volume fraction, and m represents the shape factor of the nanoparticles. The thermophysical features of Cu, CuO, and H_2O are defined in Table 1. Table 2 shows the values of the nanoparticle shape factor. Moreover, copper (Cu) and copper oxide (CuO) nanoparticles have a broad range of applications across various fields due to their excellent thermal, electrical, and chemical properties. In electronics, they are used in conductive inks, printed circuits, and semiconductors. Cu and CuO also serve as effective catalysts for chemical reactions and environmental remediation. In thermal systems, they enhance the heat transfer in nanofluids for industrial cooling and energy devices. Their antimicrobial properties make them valuable for coatings, textiles, and water purification. In biomedical applications, they have been explored for drug delivery, biosensing, and cancer therapy due to their biocompatibility and surface reactivity.

Table 1: Thermophysical features of H_2O, Cu, and CuO [59,63]

Physical property	H_2O	Cu	CuO
ρ [kg/m^3]	997.1	8,933	6,320
C_p [J/kg K]	4,179	385	531.8
k [W/m K]	0.613	401	76.5
σ [S/m]	5.5×10^{-6}	5.96×10^{7}	2.7×10^{-8}

Similarity variables are given as

$$u = bxf'(\eta), \quad v = -\sqrt{b\nu_f}\, f(\eta), \quad \theta(\eta) = \frac{T - T_\infty}{T_w - T_\infty}, \quad \eta = y\sqrt{\frac{b}{\nu_f}}. \tag{10}$$

In Eq. (10), u, v represents the velocity components along the x- and y-directions, respectively. $\theta(\eta)$ is the dimensionless temperature, defined as $\frac{T-T_\infty}{T_w-T_\infty}$, where T is the temperature, T_w is the surface temperature, and T_∞ is the free-stream temperature. Further, η is the similarity variable, defined as $y\sqrt{\frac{b}{\nu_f}}$, where y is the spatial coordinate perpendicular to the flow, b is the constant, and ν_f is the kinematic viscosity. The similarity variable η is introduced to reduce the partial differential equations to ordinary differential equations (ODEs).

Using these similarity variables, Eqs (2)–(4) are reduced to

$$\frac{\alpha_1}{\alpha_2}f'''(\eta) - (f'(\eta))^2 + f(\eta)f''(\eta) - \frac{\alpha_3}{\alpha_2}M\sin^2(\gamma)f'(\eta) - \frac{\alpha_1}{\alpha_2}Kf'(\eta) = 0, \tag{11}$$

$$\frac{1}{\alpha_5}(\alpha_4 + \mathrm{Rd})\theta''(\eta) + \frac{\mathrm{Pr}}{\alpha_5}(f(\eta)\theta'(\eta) + \alpha_1 \mathrm{Ec}M\sin^2(\gamma)(f'(\eta))^2 + Q_{\mathrm{Exp}}e^{(-n\eta)} + Q_I\theta(\eta)) = 0, \tag{12}$$

with the following conditions:

Table 2: Shape factor values of the nanoparticles [64,65]

Shapes	Sphere	Tetrahedron	Hexahedron	Lamina	Column
m	3	4.0613	3.7221	16.1576	6.3698

$$f(0) = 0, \quad f'(0) = 1 + \delta_1 f''(0), \quad f'(\infty) \to 0, \\ \theta(0) = 1 + \delta_2 \theta'(0), \quad \theta(\infty) \to 0. \tag{13}$$

In the above equations, M is the magnetic factor, K is the porosity factor, Rd represents the thermal radiation factor, Pr represents the Prandtl number, Ec represents the Eckert number, Q_{Exp} represents the exponential heat source, Q_I represents the thermal-dependent heat source, δ_1 is the velocity slip factor, and δ_2 represents the temperature slip factor. These factors are defined as follows:

$$\left.\begin{aligned} &\alpha_1 = \frac{\mu_{\text{nf}}}{\mu_{\text{f}}}, \quad \alpha_2 = \frac{\rho_{\text{nf}}}{\rho_{\text{f}}}, \quad \alpha_3 = \frac{\sigma_{\text{nf}}}{\sigma_{\text{f}}}, \quad \alpha_4 = \frac{k_{\text{nf}}}{k_{\text{f}}}, \\ &\alpha_5 = \frac{(\rho C_{\text{p}})_{\text{nf}}}{(\rho C_{\text{p}})_{\text{f}}}, \quad M = \frac{\sigma_{\text{f}} B_0^2}{b\rho_{\text{f}}}, \quad K = \frac{\mu_{\text{f}}}{b\rho_{\text{f}} K_{\text{p}}}, \\ &Q_{\text{Exp}} = \frac{Q_t}{b(\rho C_{\text{p}})_{\text{f}}}, \text{Ec} = \frac{u_w^2}{(C_{\text{p}})_{\text{f}}(T_w - T_\infty)}, \\ &\text{Pr} = \frac{\nu_{\text{f}}(\rho C_{\text{p}})_{\text{f}}}{k_{\text{f}}}, \quad \delta_1 = \sigma_1\sqrt{\frac{b}{\nu_{\text{f}}}}, \quad \delta_2 = \sigma_2\sqrt{\frac{b}{\nu_{\text{f}}}}, \\ &\text{Rd} = \frac{16\sigma^* T_\infty^3}{3k^* k_{\text{f}}}, \quad Q_I = \frac{Q_e}{b(\rho C_{\text{p}})_{\text{f}}}. \end{aligned}\right\} \tag{14}$$

The skin friction (C_{fx}) and local Nusselt number (Nu_x) are given as:

$$C_{fx} = \frac{\tau_w}{\rho_{\text{f}}(u_w(x))^2}, \quad \text{Nu}_x = \frac{x q_w}{k_{\text{f}}(T_w - T_\infty)}, \tag{15}$$

with

$$\tau_w = \mu_{\text{nf}} \left.\frac{\partial u}{\partial y}\right|_{y=0}, \\ q_w = -k_{\text{nf}} \left(\left.\frac{\partial T}{\partial y}\right|_{y=0} - \frac{16\sigma^*}{3k^*} \left.\frac{\partial T^4}{\partial y}\right|_{y=0} \right). \tag{16}$$

Thus, Eq. (15) is reduced to

$$C_{\text{f}} = \sqrt{\text{Re}_x} C_{fx} = \alpha_1 f''(0), \quad \frac{\text{Nu}_x}{\sqrt{\text{Re}_x}} = -(\alpha_4 + \text{Rd})\theta'(0), \tag{17}$$

where $\text{Re}_x = \frac{bx^2}{\nu_{\text{f}}}$ is the Reynolds number (local).

3 Numerical solution

Eqs (11) and (12) are highly nonlinear, so to solve them with the boundary conditions given in Eq. (13), the bvp4c technique is used. It is a numerical approach that is widely used to evaluate boundary value problems in the field of computational mathematics and engineering. In addition, it offers the advantage of efficiently handling complex boundary conditions and nonlinearities, making it a valuable tool in scientific computing and engineering analysis. To ensure the accuracy of the applied numerical technique, an error tolerance of 10^{-6} was applied. This value is sufficiently small to minimize the numerical error and confirm the convergence and stability of the solution. To apply this technique, the given higher-order ODEs must be converted into first-order ODEs. Therefore, we assume that

$$f = \chi(1), \quad f' = \chi(2), \quad f'' = \chi(3), \quad f''' = \chi'(3), \\ \theta = \chi(4), \quad \theta' = \chi(5), \quad \theta'' = \chi'(5). \tag{18}$$

Using Eq. (18), Eqs (11) and (12) along with Eq. (13) are transformed as

$$\chi'(3) = -\left\{ \frac{\chi(1)\chi(3) - (\chi(2))^2 - \frac{\alpha_3}{\alpha_2} M \sin^2\gamma\chi(2) - \frac{\alpha_1}{\alpha_2} K\chi(2)}{\frac{\alpha_1}{\alpha_2}} \right\}, \tag{19}$$

$$\chi'(5) = -\left\{ \frac{\frac{\text{Pr}}{\alpha_5}(\chi(1)\chi(5) + \alpha_1 \text{Ec} M \sin^2\gamma(\chi(2))^2 + Q_{\text{Exp}} e^{(-n\eta)} + Q_I\chi(4))}{\frac{1}{\alpha_5}(\alpha_4 + \text{Rd})} \right\}, \tag{20}$$

and

$$\chi_{\text{initial}}(1) - 0, \quad \chi_{\text{initial}}(2) - \{1 + \delta_1\chi_{\text{initial}}(3)\}, \\ \chi_{\text{boundary}}(2) - 0, \\ \chi_{\text{initial}}(4) - \{1 + \delta_2\chi_{\text{initial}}(5)\}, \quad \chi_{\text{boundary}}(4) - 0. \tag{21}$$

4 Validation

To confirm the validation of the current study, a comparative analysis is carried out in Table 2 that matches current results with established works of Hamad [66], Wang [67], and Reddy Gorla and Sidawi [68]. By varying the values of the Prandtl number while keeping all the other factors at zero, a fine agreement has been noticed in this table that ensures the validation of the current study (Table 3).

5 Results and discussion

This study investigates thermally radiative nanofluids flowing over a porous surface. The flow dynamics are affected by the collective impacts of exponential and thermal-dependent heat sources. Additionally, an inclined

Table 3: Comparison of the current and published results when all other factors are zero

Pr	0.07	0.2	0.7	2	7	20	70
Hamad [66]	0.06556	0.16909	0.45391	0.91136	1.8954	3.3539	6.4622
Wang [67]	0.0656	0.1691	0.4539	0.9114	1.8954	3.3539	6.4622
Reddy Gorla and Sidawi [68]	0.0656	0.1691	0.4539	0.9114	1.8954	3.3539	6.4622
Present results	0.065571	0.169089	0.45391	0.911363	1.895413	3.353802	6.462193

magnetic effect is introduced to the flow system. The velocity and thermal slip conditions are imposed to investigate the nanofluid velocity and temperature distributions. The bvp4c Matlab built-in function is used to solve the modeled problem. The influences of various factors on velocity and thermal profiles are discussed in Figures 2–17 and Tables 4–15. The default values of factors are considered as $1.0 \le K \le 3.0$, $1.0 \le M \le 3.0$, $30^\circ \le \gamma \le 90^\circ$, $0.1 \le \delta_1 \le 0.5$, $0.1 \le \mathrm{Ec} \le 0.5$, $0.1 \le \delta_2 \le 0.5$, $0.1 \le Q_{\mathrm{Exp}} \le 0.5$, $0.1 \le Q_I \le 0.5$, and $0.1 \le \mathrm{Rd} \le 0.5$.

5.1 Velocity distributions

The impressions of diverse factors on velocity distributions ($f(\eta)$, $f'(\eta)$) are depicted in Figures 2–4. Figure 2(a) and (b)

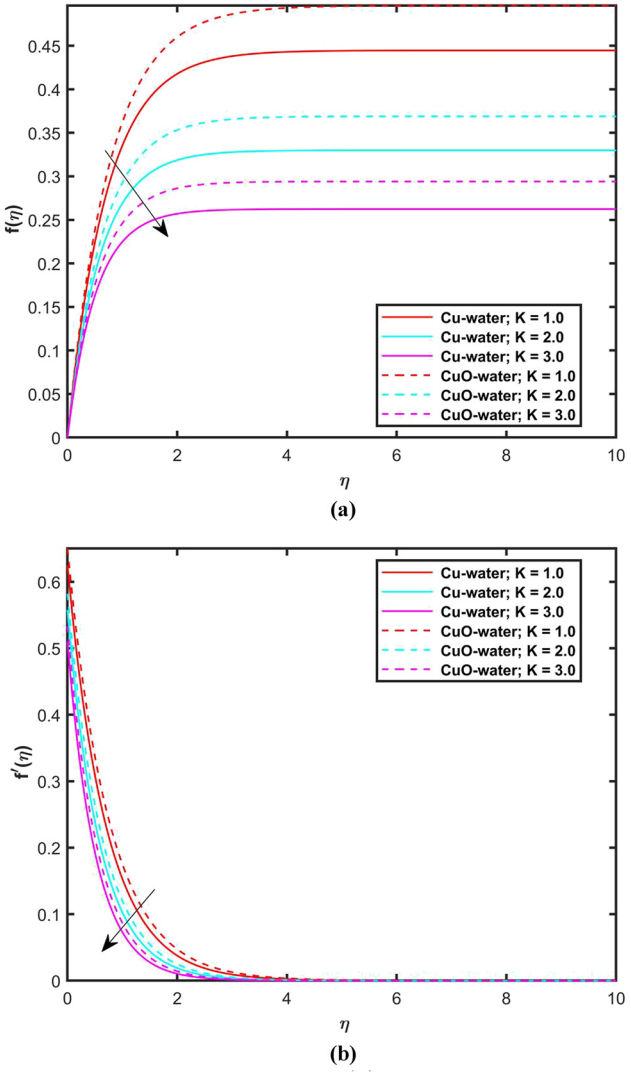

Figure 2: (a) and (b) Behavior of $f(\eta)$ and $f'(\eta)$ against K.

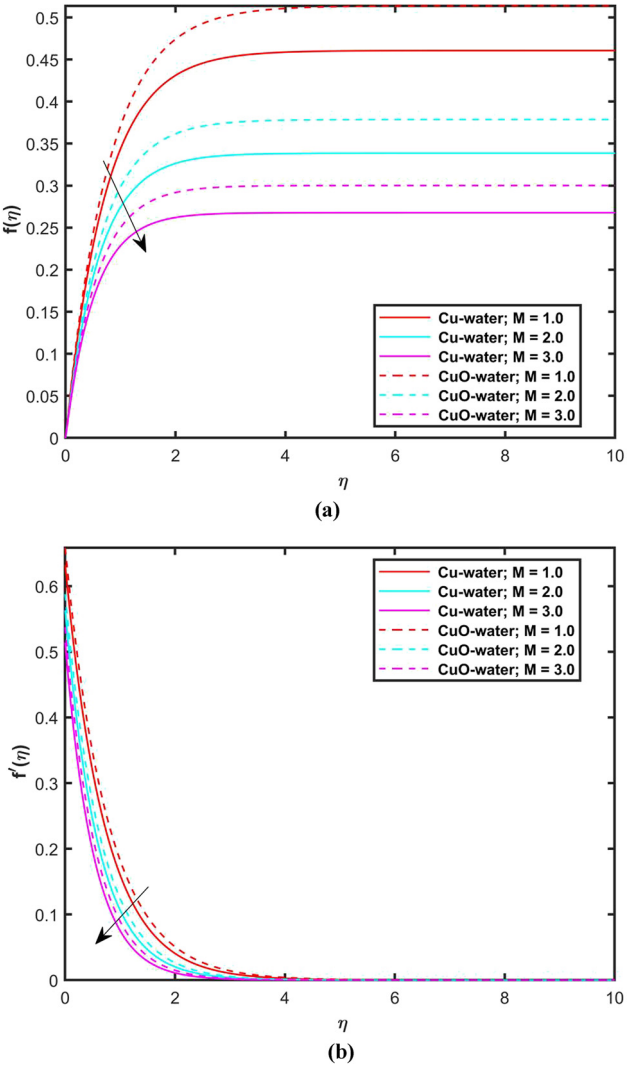

Figure 3: (a) and (b) Behavior of $f(\eta)$ and $f'(\eta)$ against M.

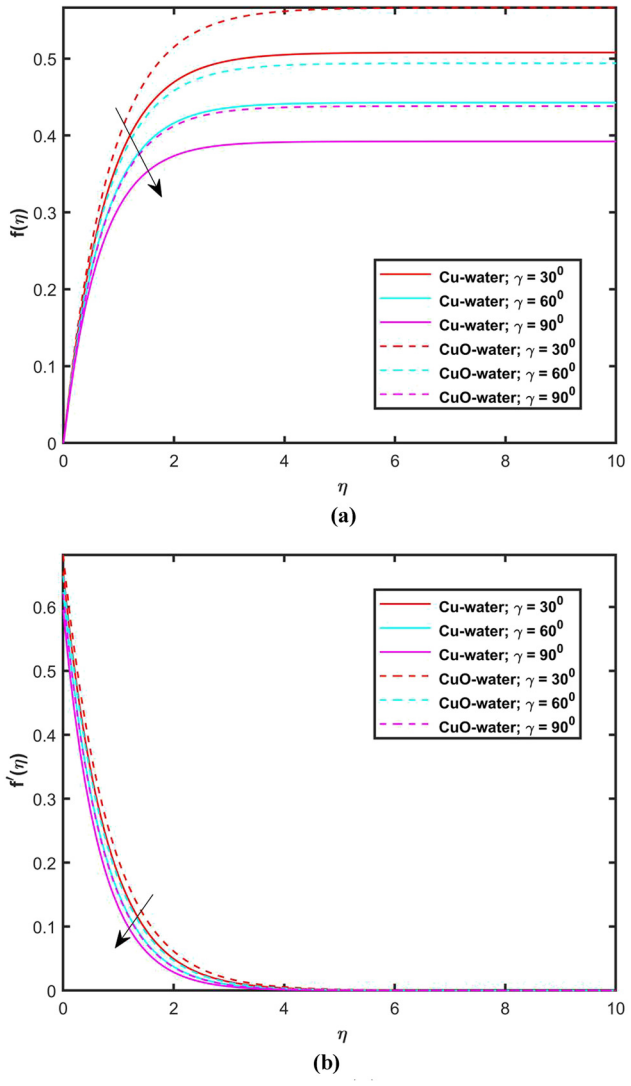

Figure 4: (a) and (b) Behavior of $f(\eta)$ and $f'(\eta)$ against γ.

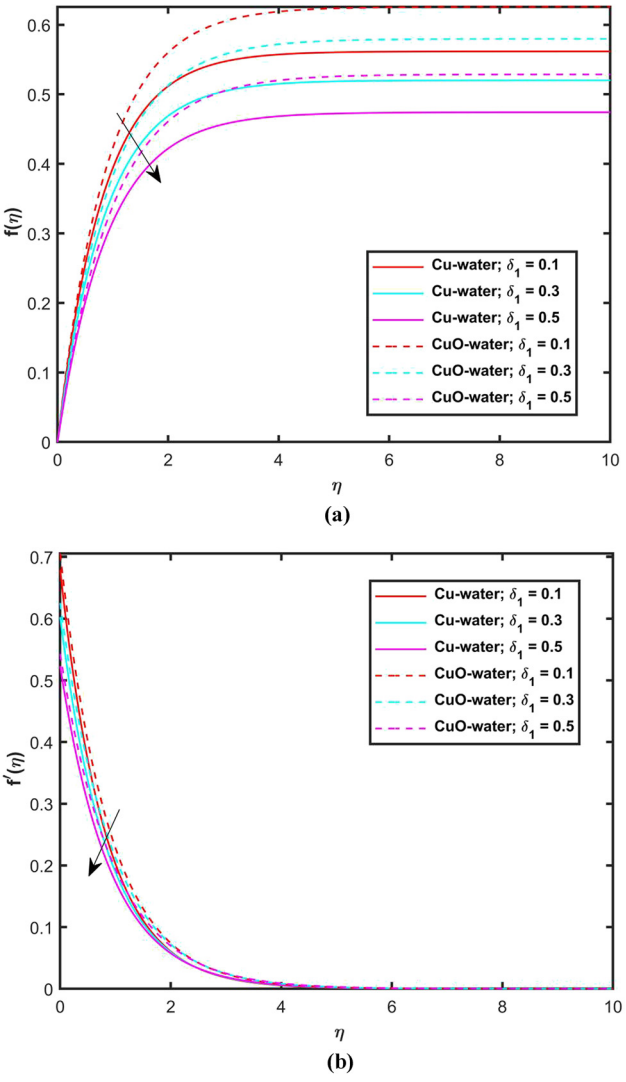

Figure 5: (a) and (b) Behavior of $f(\eta)$ and $f'(\eta)$ against δ_1.

shows the impression of the porosity factor (K) on ($f(\eta)$, $f'(\eta)$). Here, we observed that the greater K reduces both $f(\eta)$ and $f'(\eta)$. Actually, the introduction of porous behavior on the stretching surface signifies an increase in the surface's effective permeability due to the presence of expanding pores. This augmentation in porosity facilitates the passage of fluid through the surface, thereby increasing the resistance encountered by the flowing fluid. When the resistance force increases with increasing porosity factor, the velocity profiles reduce as a result. From the obtained results in Figure 2(a) and (b), it is seen that the porous factor affects the CuO–water nanofluid flow more than the Cu–water nanofluid flow. Actually, the changes in the porous structure have a stronger impact on the flow behavior of CuO–water compared to Cu–water. This is due to the differences in physical properties like viscosity,

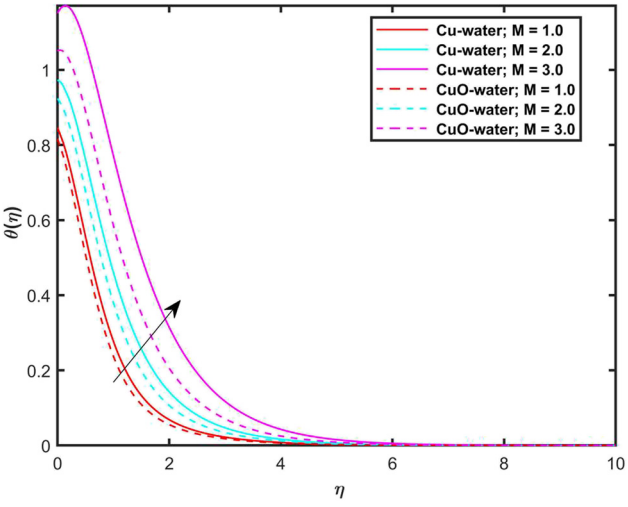

Figure 6: Behavior of $\theta(\eta)$ against M.

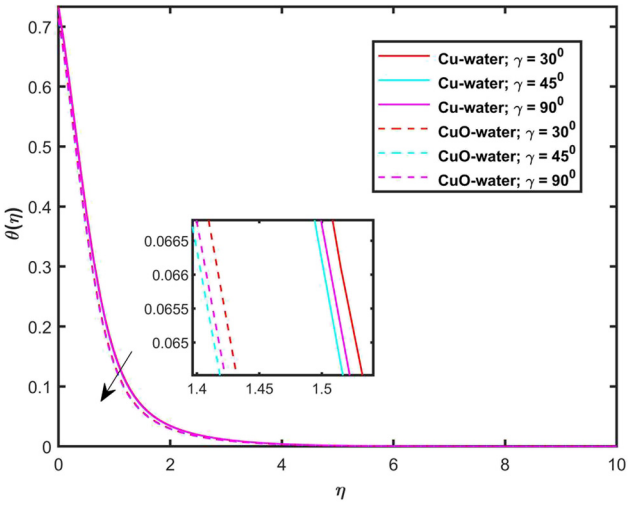

Figure 7: Behavior of $\theta(\eta)$ against γ.

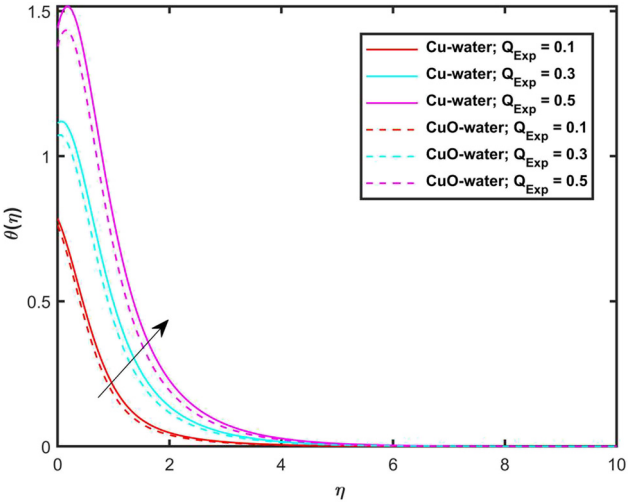

Figure 10: Behavior of $\theta(\eta)$ against Q_{Exp}.

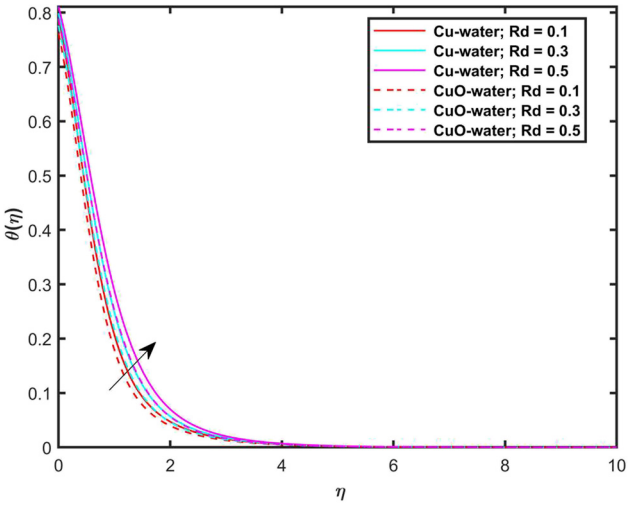

Figure 8: Behavior of $\theta(\eta)$ against Rd.

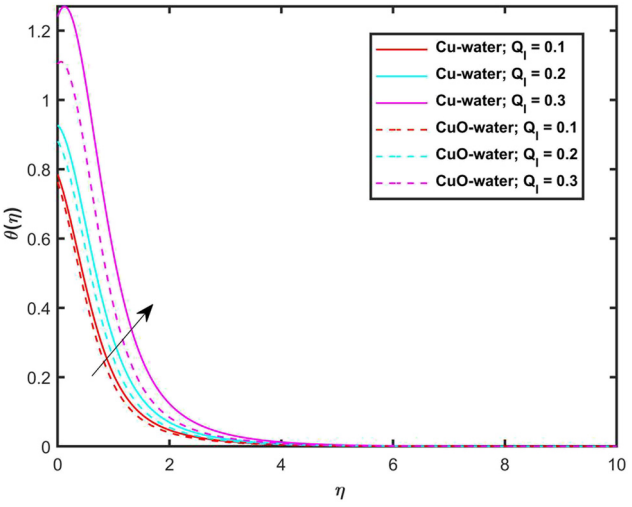

Figure 11: Behavior of $\theta(\eta)$ against Q_I.

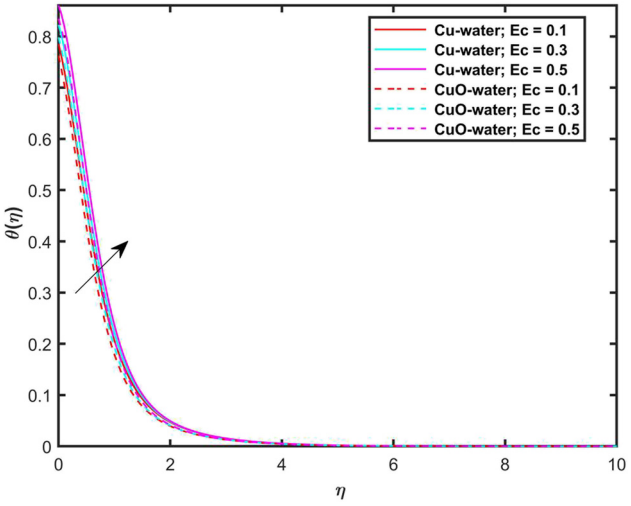

Figure 9: Behavior of $\theta(\eta)$ against Ec.

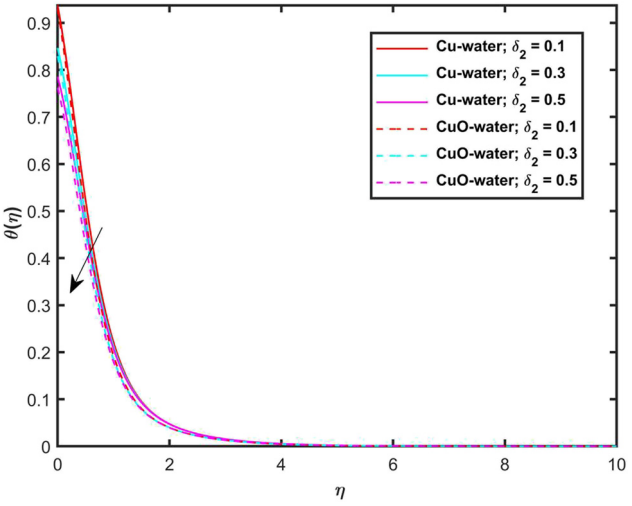

Figure 12: Behavior of $\theta(\eta)$ against δ_2.

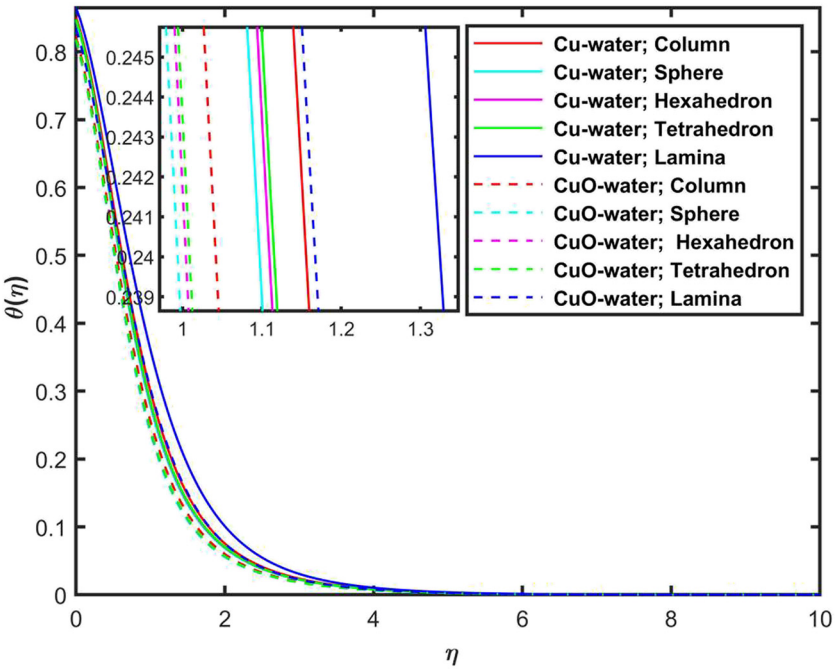

Figure 13: Variations in temperature distributions of the Cu–water and CuO–water nanofluids flows with different shapes of Cu and CuO nanoparticles.

thermal conductivity, or particle concentration between the two nanofluids. As a result, the CuO–water nanofluid experiences more noticeable changes in velocity or flow pattern when the porosity factor is varied, indicating a higher sensitivity to the medium's structure. Figure 3(a) and (b) demonstrates the variation in $f(\eta)$ and $f'(\eta)$ *via* greater M. The increase in M implies a stronger impact of magnetic force on the nanofluid flow. Physically, this can be understood as the magnetic field imposing resistance on the nanofluid flow, effectively impeding its motion. As M

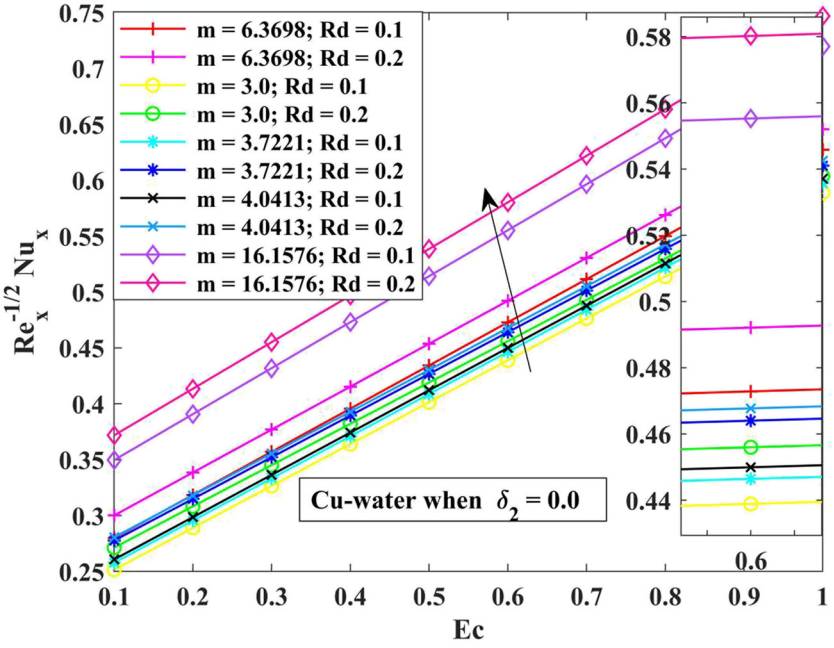

Figure 14: Variations in the Nusselt number ($\mathrm{Re}_x^{-1/2}\,\mathrm{Nu}_x$) *via* Rd and Ec in the case of Cu–water nanofluid flow when $\delta_2 = 0.0$.

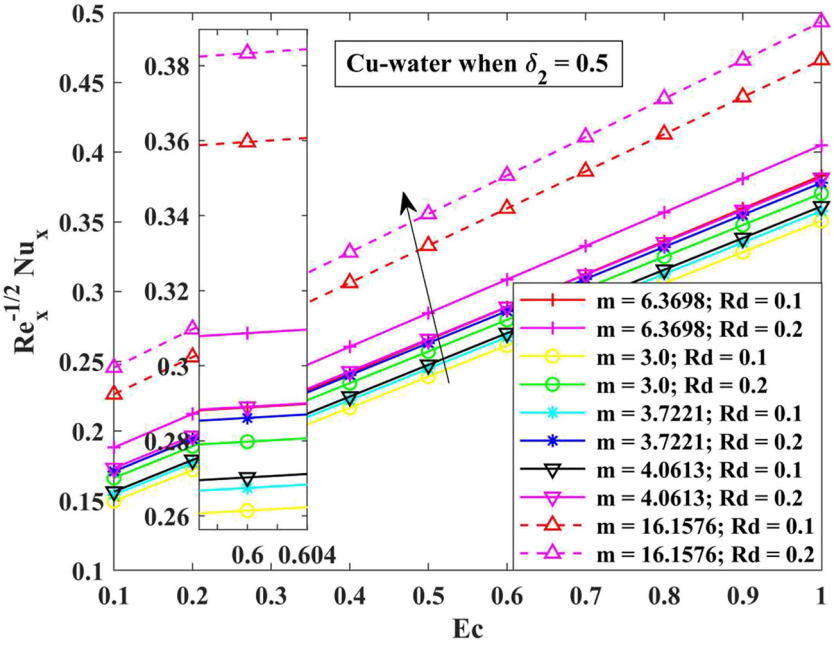

Figure 15: Variations in the Nusselt number ($Re_x^{-1/2} Nu_x$) *via* Rd and Ec in the case of Cu–water nanofluid flow when $\delta_2 = 0.5$.

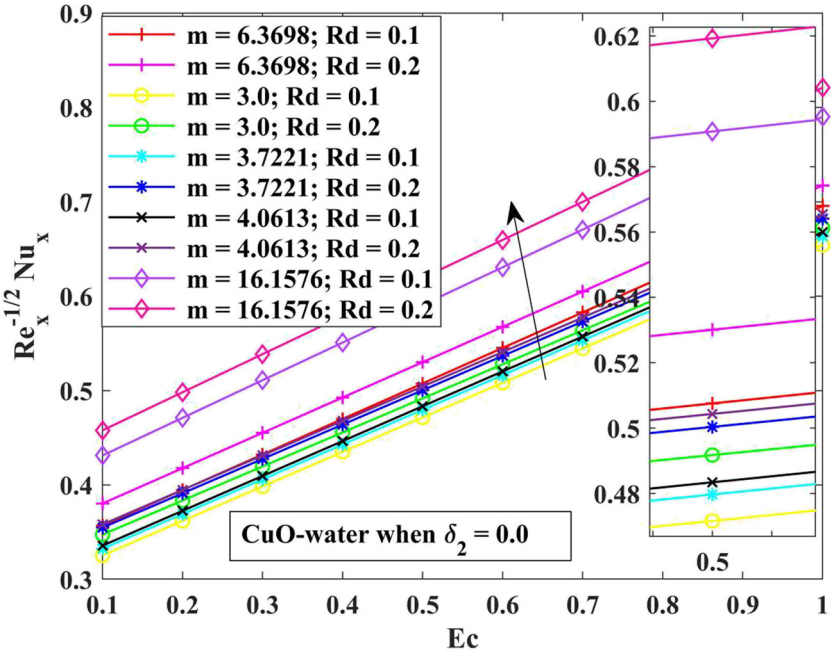

Figure 16: Variations in the Nusselt number ($Re_x^{-1/2} Nu_x$) *via* Rd and Ec in the case of CuO–water nanofluid flow when $\delta_2 = 0.0$.

increases, the intensity of this resistance increases, causing a reduction in $f(\eta)$ and $f'(\eta)$. This phenomenon arises from the association between the magnetic field and the fluid's magnetic susceptibility, leading to alteration in the fluid's momentum distribution and ultimately slowing down its movement. Hence, the increase in M directly correlates with a decrease in fluid velocities, reflecting the significant impact of the magnetic force on the nanofluid flow behavior. When comparing the Cu–H_2O nanofluid to the CuO–H_2O nanofluid, the presence of CuO nanoparticles alters the fluid's magnetic susceptibility and interaction with the applied magnetic field effect. This alteration results in a less significant decrease in the velocity of the CuO–H_2O nanofluid compared to the Cu–H_2O

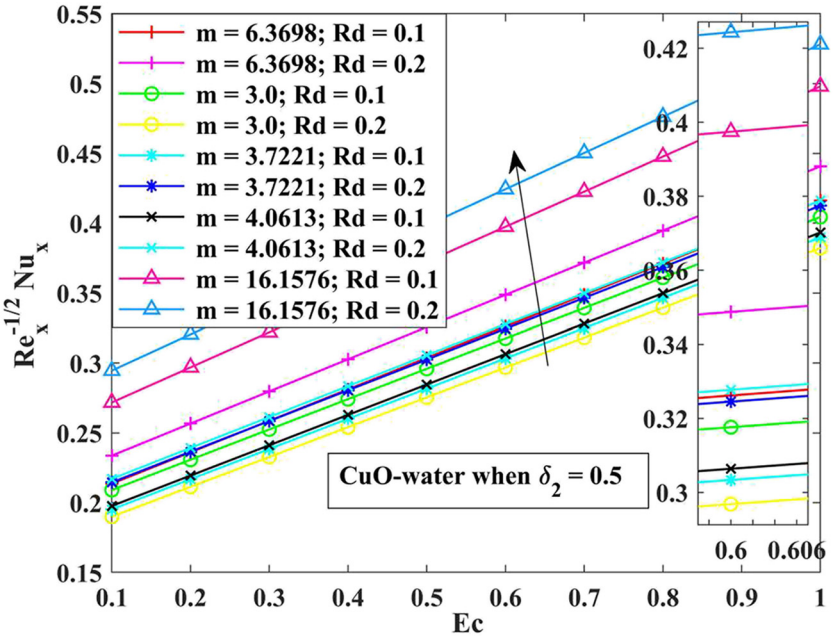

Figure 17: Variations in the Nusselt number ($Re_x^{-1/2} Nu_x$) *via* Rd and Ec in the case of CuO–water nanofluid flow when $\delta_2 = 0.5$.

nanofluid. Physically, this suggests that the magnetic field exerts a more noticeable decelerating consequence on the Cu–H_2O nanofluid flow because of its higher magnetic susceptibility, leading to greater resistance against the stretching motion of the surface. Conversely, the occurrence of CuO nanoparticles in the nanofluid mitigates this effect to some extent, resulting in a relatively smaller reduction in $f(\eta)$ and $f'(\eta)$, as shown in Figure 4(a) and (b). These figures validate that the velocities $f(\eta)$ increase with an increase in γ. The increase in γ corresponds to a change in the direction of the magnetic force acting on the nanofluid flow along a stretching surface. Physically, this alteration in γ distresses how the magnetic field interrelates with the nanofluid, potentially enhancing the stretching and alignment of the fluid flow. As γ increases, the magnetic field experiences a better influence by the nanofluid flow, thereby promoting more declining velocity of the nanofluid flows. From the obtained results, it was found that the magnetic field influenced the nanofluid flows more when the angle was 90°. We call this type of applied magnetic field the transverse magnetic field. It was also found that velocity panels of the Cu-H_2O nanofluid flow are greatly influenced by higher M because the electrical conductivity of the Cu nanoparticles is better than that of CuO nanoparticles. Figure 5(a) and (b) demonstrates the variation in $f(\eta)$ and $f'(\eta)$ *via* the velocity slip factor (δ_1). When δ_1 increases, it indicates an enhanced slip or deviation of the nanofluid velocity at the surface in comparison to the no-slip condition. This slip implies that the fluid molecules close to the surface move faster or slower than the surface itself, resulting in a reduction in $f(\eta)$ and $f'(\eta)$.

5.2 Thermal distribution

The effects of numerous factors on the thermal distribution $\theta(\eta)$ are shown in Figures 6–12. Figure 6 illustrates the

Table 4: Impact of Ec on the heat transfer rate of the Cu–water nanofluid when $\delta_2 = 0.0$

Shapes → Parameter ↓	Column	Sphere	Hexahedron	Tetrahedron	Lamina
Ec	m = 6.3698	m = 3.0	m = 3.7221	m = 4.0613	m = 16.1576
0.1	0.5500258982	0.5138053375	0.5218766181	0.5256075260	0.6375105888
0.2	0.5886142049	0.5512667758	0.5595940538	0.5634423141	0.6786305709
0.3	0.6272024650	0.5887282147	0.5973114896	0.6012770126	0.7197530617

Table 5: Impact of Ec on the heat transfer rate of the Cu-water nanofluid when $\delta_2 = 0.5$

Shapes → Parameter ↓	Column	Sphere	Hexahedron	Tetrahedron	Lamina
Ec	$m = 6.3698$	$m = 3.0$	$m = 3.7221$	$m = 4.0613$	$m = 16.1576$
0.1	0.5321828479	0.4848875669	0.4952485750	0.5000721469	0.6557037633
0.2	0.5379987284	0.4902938818	0.5007457063	0.5056113427	0.6625367868
0.3	0.5438183911	0.4957002029	0.5062428434	0.5111505442	0.6693698102

Table 6: Impact of Rd on the heat transfer rate of the Cu–water nanofluid when $\delta_2 = 0.0$

Shapes → Parameter ↓	Column	sphere	Hexahedron	Tetrahedron	Lamina
Rd	$m = 6.3698$	$m = 3.0$	$m = 3.7221$	$m = 4.0613$	$m = 16.1576$
0.1	0.6272024650	0.5887282147	0.5973114896	0.6012770126	0.7197530617
0.2	0.6456752125	0.6037442552	0.6130896798	0.6174042117	0.7468879188
0.3	0.6625485083	0.6175992852	0.6276058922	0.6322336027	0.7715460232

impact of the magnetic factor (M) on $\theta(\eta)$. This augmentation in $\theta(\eta)$ can be understood as a result of the enhanced energy dissipation due to the increased magnetic forces acting on the fluid particles. Essentially, a higher M imposes resistance on the nanofluid motion, causing increased frictional heating and thereby elevating the temperature gradient. For the Cu–H_2O nanofluid matched with the CuO–H_2O nanofluid, the occurrence of Cu nanoparticles modifies the thermal properties of the nanofluid, leading to a more significant augmentation in the temperature distribution, as depicted in Figure 6. Physically, this can be attributed to the heightened heat transfer capabilities of the nanofluid in the presence of nanoparticles, which interact with the magnetic field to facilitate more efficient heat dissipation. Figure 7 illustrates that $\theta(\eta)$ declines with an increase in the angle of inclination (γ). When γ increases, it implies a deviation of the magnetic lines of force from being perpendicular to the surface. This adjustment reduces the effective strength of the magnetic field acting parallel to surface, which, in turn, diminishes the induced Lorentz force exercised on the fluid; consequently, the decrease in the frictional heating and thermal transfer within the nanofluid causes a reduction in $\theta(\eta)$. Physically, this can be interpreted as a smaller (M) influence on fluid dynamics, resulting in a less pronounced impact on temperature gradients and decrease in $\theta(\eta)$. Figure 8 shows that $\theta(\eta)$ augments with an increase in the radiation factor (Rd). When Rd increases, it indicates a better rate of energy transmission from the surface to the surrounding fluid. This enhanced radiation results in amplified thermal transfer from the surface, which subsequently increases $\theta(\eta)$. Physically, the augmentation in $\theta(\eta)$ can be understood as a result of greater thermal energy loss from the system, leading to a more rapid depletion of the heat available to the nanofluid. For the Cu–H_2O nanofluid matched with the CuO–H_2O nanofluid, the presence of Cu nanoparticles modifies the thermal properties of the fluid, causing augmentation in the temperature profile, as shown in Figure 8. Figure 9 shows that $\theta(\eta)$ augments with an increase in the Eckert number (Ec). When Ec increase, it implies a higher ratio of kinetic energy to enthalpy change in the nanofluid flow. This signifies that more of the energy

Table 7: Impact of Rd on the heat transfer rate of the Cu–water nanofluid when $\delta_2 = 0.5$

Shapes → Parameter ↓	Column	Sphere	Hexahedron	Tetrahedron	Lamina
Rd	$m = 6.3698$	$m = 3.0$	$m = 3.7221$	$m = 4.0613$	$m = 16.1576$
0.1	0.4479725362	0.4097581918	0.4181507221	0.4445721225	0.5467894505
0.2	0.4739733867	0.4331093030	0.4420774964	0.4703341655	0.5799366421
0.3	0.4985422898	0.4551437556	0.4646645597	0.4946750448	0.6113375818

Table 8: Impact of M on the heat transfer rate of the Cu–water nanofluid when $\delta_2 = 0.0$

Shapes → Parameter ↓	Column	Sphere	Hexahedron	Tetrahedron	Lamina
M	m = 6.3698	m = 3.0	m = 3.7221	m = 4.0613	m = 16.15760
0.1	0.6879867431	0.6456006690	0.6550379169	0.6594016178	0.7910766290
0.2	0.7196352530	0.6752505076	0.6851251604	0.6896926205	0.8280855561
0.3	0.7522465074	0.7058272617	0.7161476742	0.7209226719	0.8661410723

provided to the system is transformed into kinetic energy rather than being absorbed as heat. Consequently, with the higher Ec, the flow carries more kinetic energy, which leads to increased heat transfer. This augmentation in $\theta(\eta)$ is a result of enhanced energy dissipation, where a better portion of flow energy is altered to thermal energy due to heightened fluid motion. In the case of the Cu–water nanofluid compared to the CuO–water nanofluid, the presence of Cu nanoparticles modifies the thermal properties of the fluid, leading to a more significant augmentation in temperature distribution, as depicted in Figure 9. Figure 10 shows that $\theta(\eta)$ augments with an increase in the exponential heat source factor (Q_{Exp}). When the exponential heat source factor increases, it implies a higher rate of heat generation within the fluid due to an exponential increase in the heat source. This additional heat input contributes to an augmentation in $\theta(\eta)$. Physically, the increase in Q_{Exp} results in more energy being released into the fluid, causing heightened thermal energy dissipation and subsequently higher temperatures within the nanofluid flow domain. In the case of Cu–water nanofluid compared to the CuO–water nanofluid, the presence of Cu nanoparticles modifies the thermal properties of the fluid, causing better augmentation in $\theta(\eta)$, as depicted in Figure 10. Figure 11 shows that $\theta(\eta)$ increase with an increase in (Q_I). When Q_I increases, then heat generation within the nanofluid is directly influenced by its temperature. As the temperature of the nanofluid increases, the heat source factor also increases, leading to a higher temperature distribution. This increase in Q_I leads to an increase in $\theta(\eta)$. In the case of Cu–water nanofluid compared to the CuO–water nanofluid, the presence of Cu nanoparticles modifies the thermal properties of the fluid, causing a more substantial augmentation in temperature distribution, as depicted in Figure 11. Figure 12 shows that $\theta(\eta)$ declines with an increase in the thermal slip factor (δ_2). When δ_2 increases, it indicates an enhanced ability of the fluid molecules to exchange heat with the surface. This means that the fluid molecules can more effectively transfer thermal energy across the boundary layer, resulting in a reduction in $\theta(\eta)$. Physically, an increase in δ_2 promotes more efficient heat transfer, allowing the nanofluid to carry away heat

Table 9: Impact of M on the heat transfer rate of the Cu–water nanofluid when $\delta_2 = 0.5$

Shapes → Parameter ↓	Column	Sphere	Hexahedron	Tetrahedron	Lamina
M	m = 6.3698	m = 3.0	m = 3.7221	m = 4.0613	m = 16.15760
0.1	0.5024227430	0.4583517342	0.4680202806	0.4725188871	0.6166583180
0.2	0.5229628390	0.4768784077	0.4869819136	0.4916842033	0.6428619407
0.3	0.5438183911	0.4957002029	0.5062428434	0.5111505442	0.6693698102

Table 10: Impact of Ec on the heat transfer rate of the CuO–water nanofluid when $\delta_2 = 0.0$

Shapes → Parameter ↓	Column	Sphere	Hexahedron	Tetrahedron	Lamina
Ec	m = 6.3698	m = 3.0	m = 3.7221	m = 4.0613	m = 16.1576
0.1	0.8902787300	0.8263632989	0.8407061367	0.8473165342	1.040542310
0.2	0.8989690336	0.8345874477	0.8490357722	0.8556944761	1.050252470
0.3	0.9076531895	0.8428115964	0.8573654077	0.8640723984	1.059962631

Table 11: Impact of Ec on the heat transfer rate of the CuO–water nanofluid when $\delta_2 = 0.5$

Shapes → Parameter ↓	Column	Sphere	Hexahedron	Tetrahedron	Lamina
Ec	$m = 6.3698$	$m = 3.0$	$m = 3.7221$	$m = 4.0613$	$m = 16.1576$
0.1	0.5687866175	0.5202281081	0.5310228273	0.5360177574	0.6875476919
0.2	0.5743359023	0.5254064073	0.5362841482	0.5413177023	0.6939637512
0.3	0.5798860422	0.5305829422	0.541545469	0.5466176383	0.7003798104

more efficiently and, consequently, the temperature gradient along the stretching surface decreases. Figure 13 depicts that the temperature distribution has different behaviors against the different shapes of nanoparticles. There is maximum growth in $\theta(\eta)$ for the lamina-shaped nanoparticles. In the case of lamina-shaped nanoparticles, there tends to be a maximum increase in thermal flow. This is because lamina-shaped nanoparticles typically have a larger surface area compared to other shapes for the same volume, which promotes greater interaction with the surrounding nanofluid. As a result, lamina-shaped nanoparticles can effectively enhance heat transfer by increasing the contact area between the fluid and the nanoparticles. This increased surface area facilitates more efficient heat exchange, leading to a higher rate of thermal energy transfer and consequently a greater augmentation in temperature distribution within the nanofluid flow. Therefore, in systems where effective heat transfer is desired, the presence of lamina-shaped nanoparticles can significantly influence and maximize the thermal flow behavior. Again in the case of Cu–water nanofluid compared to the CuO–water nanofluid, the presence of Cu nanoparticles modifies the thermal properties of the fluid, leading to a more significant augmentation in $\theta(\eta)$, as depicted in Figure 13.

5.3 Nusselt number

Figures 14 and 15 depict that $\mathrm{Re}_x^{-1/2}\mathrm{Nu}_x$ increases with an increase in the radiation factor (Rd) and Eckert number (Ec) when $\delta_2 = 0.0$ and $\delta_2 = 0.5$ for the Cu–water nanofluid. As Rd increases, it indicates that radiative heat transfer becomes more significant in contributing to the overall heat transfer process. This augmentation in $\mathrm{Re}_x^{-1/2}\mathrm{Nu}_x$ suggests that the convective heat transfer is enhanced due to the additional heat transfer mechanism introduced by radiation. Furthermore, the higher heat transfer rate is found for lamina-shaped nanoparticles in the presence and absence of thermal slip conditions. Figures 16 and 17 depict that $\mathrm{Re}_x{}^{-1/2}\,\mathrm{Nu}_x$ augments with an increase in Rd and Ec when $\delta_2 = 0.0$ and $\delta_2 = 0.5$ for the CuO–water nanofluid. This trend suggests that increasing Rd enhances the radiative heat transfer contribution, while increasing Ec augments the convective heat transfer. In the case of $\delta_2 = 0.5$, where there is a relative slip between the fluid and surface, the Nusselt number further increases due to enhanced fluid mixing and increased convective heat transfer. Under no-slip conditions, $\mathrm{Re}_x^{-1/2}\mathrm{Nu}_x$ still increases with Ec, indicating that convective heat transfer dominates despite the absence of slip. These trends highlight the combined influence of radiation and convective heat transfer mechanisms on heat transfer enhancement in the CuO–water nanofluid. Furthermore, the higher heat transfer rate is found for lamina-shaped nanoparticles in the presence and absence of thermal slip conditions.

5.4 Table discussion

The impacts of various factors on $\mathrm{Re}_x^{-1/2}\mathrm{Nu}_x$ regarding Cu–water and CuO–water nanofluids are depicted in

Table 12: Impact of Rd on the heat transfer rate of the CuO–water nanofluid when $\delta_2 = 0.0$

Shapes → Parameter ↓	Column	Sphere	Hexahedron	Tetrahedron	Lamina
Rd	$m = 6.3698$	$m = 3.0$	$m = 3.7221$	$m = 4.0613$	$m = 16.1576$
0.1	0.8133207011	0.7650727653	0.7759434836	0.7809461591	0.9250412488
0.2	0.8389160014	0.7858160329	0.7977718794	0.8032740654	0.9621856566
0.3	0.8631182582	0.8057018763	0.8186166398	0.8245627745	0.9968976138

Table 13: Impact of Rd on the heat transfer rate of the CuO–water nanofluid when $\delta_2 = 0.5$

Shapes → Parameter ↓	Column	Sphere	Hexahedron	Tetrahedron	Lamina
Rd	m = 6.3698	m = 3.0	m = 3.7221	m = 4.0613	m = 16.1576
0.1	0.4750996874	0.4362669660	0.4449196398	0.4489195558	0.5692057223
0.2	0.5032848123	0.4616647800	0.4709328806	0.4752183306	0.6043920095
0.3	0.5300707465	0.4857794328	0.4956366174	0.5001956787	0.6379036944

Table 14: Impact of M on the heat transfer rate of the CuO–water nanofluid when $\delta_2 = 0.0$

Shapes → Parameter ↓	Column	sphere	Hexahedron	Tetrahedron	Lamina
M	m = 6.3698	m = 3.0	m = 3.7221	m = 4.0613	m = 16.15760
0.1	0.8387346180	0.7791929008	0.7925697591	0.7987317128	0.977951303
0.2	0.8726977989	0.8105372556	0.8244957637	0.8309273315	1.018400033
0.3	0.9076531895	0.8428115964	0.8573654077	0.8640723984	1.059962631

Table 15: Impact of M on the heat transfer rate of the CuO–water nanofluid when $\delta_2 = 0.5$

Shapes → Parameter ↓	Column	Sphere	Hexahedron	Tetrahedron	Lamina
M	m = 6.3698	m = 3.0	m = 3.7221	m = 4.0613	m = 16.15760
0.1	0.5423729946	0.4965025902	0.5067094298	0.5114305183	0.6540461149
0.2	0.5609563373	0.5133812346	0.5239635359	0.5288587981	0.6770193930
0.3	0.5798860422	0.5305829422	0.5415454690	0.5466176383	0.7003798104

Tables 4–15 for both $\delta_2 = 0.0$ and $\delta_2 = 0.5$ conditions. Tables 4 and 5 show the impacts of the Eckert number (Ec)numerically on $\mathrm{Re}_x^{-1/2}\mathrm{Nu}_x$ by keeping $\delta_2 = 0.0$ and $\delta_2 = 0.5$ while all other factors as fixed. It was observed from these tables that when $\delta_2 = 0.0$, the values of $\mathrm{Re}_x{}^{-1/2}\,\mathrm{Nu}_x$ increase more quickly for lamina-shaped nanoparticles with variation in Ec. Tables 6 and 7 show the impacts of the radiation factor Rd numerically on $\mathrm{Re}_x^{-1/2}\mathrm{Nu}_x$ by keeping $\delta_2 = 0.0$ and $\delta_2 = 0.5$, while all other factors are fixed. It was observed from these tables that when $\delta_2 = 0.0$, the values of $\mathrm{Re}_x^{-1/2}\mathrm{Nu}_x$ increase more quickly for lamina-shaped nanoparticles with variation in Rd. Tables 8 and 9 show the impacts of the magnetic factor (M)numerically on $\mathrm{Re}_x^{-1/2}\mathrm{Nu}_x$ when $\delta_2 = 0.0$ and $\delta_2 = 0.5$ while all other factors are fixed. It was observed from these tables that when $\delta_2 = 0.0$, the values of $\mathrm{Re}_x^{-1/2}\mathrm{Nu}_x$ increase more quickly for lamina-shaped nanoparticles with variation in M. Tables 10 and 11 show the impacts of the Eckert number (Ec) numerically on $\mathrm{Re}_x^{-1/2}\mathrm{Nu}_x$ when $\delta_2 = 0.0$ and $\delta_2 = 0.5$ while all other factors are fixed and considering the CuO–water nanofluid. It was observed from these tables that when $\delta_2 = 0.0$, the values of $\mathrm{Re}_x^{-1/2}\mathrm{Nu}_x$ increase more quickly for lamina-shaped nanoparticles with variation in Ec. Tables 12 and 13 show the impacts of the radiation factor (Rd) numerically on $\mathrm{Re}_x^{-1/2}\mathrm{Nu}_x$ when $\delta_2 = 0.0$ and $\delta_2 = 0.5$ while all other factors are fixed and considering the CuO–water nanofluid. It was noticed from these tables that when $\delta_2 = 0.0$ the values of $\mathrm{Re}_x^{-1/2}\mathrm{Nu}_x$ increase more quickly for Lamina-shaped nanoparticles with variation in Rd. Tables 14 and 15 show the impact of the magnetic factor M numerically on $\mathrm{Re}_x^{-1/2}\mathrm{Nu}_x$ when $\delta_2 = 0.0$ and $\delta_2 = 0.5$ while all other factors are fixed, and considering the CuO–water nanofluid. It was observed from these tables that when $\delta_2 = 0.0$, the values of $\mathrm{Re}_x^{-1/2}\mathrm{Nu}_x$ increase more quickly for lamina-shaped nanoparticles with variation in M.

6 Conclusion

This study investigates thermally radiative nanofluid flows over a surface using porous media. The flow dynamics are

affected by the combined impacts of exponential and temperature-dependent heat sources. Additionally, the inclined magnetic effect was introduced to the flow system. The flow in the system is induced by the stretching nature of the sheet. The textured surface of the stretching sheet facilitates the exploration of velocity and thermal slip conditions. The impacts of different factors on the velocity, thermal skin friction, and heat transfer rate is discussed in detail. Based on the above analysis, the following conclusions are drawn.

- As the porosity factor, velocity slip factor, and magnetic factor increase, they impose greater resistance on the fluid flow, leading to a decline in the velocity distributions. The reduction is more pronounced in Cu–water nanofluid due to the stronger resistive effects, such as higher density and stronger magnetic interaction, which impede the flow.
- CuO–water nanofluids experience relatively less resistance because of the lower density and better stability of CuO nanoparticles, allowing them to maintain higher velocities with an increase in the porosity factor, velocity slip factor, and magnetic factor.
- Both velocity distributions decline with increasing values of inclination angle with respect to the magnetic field effects. Moreover, these velocities are maximum when the angle of inclination is 90°. This occurs because the magnetic field's impact on the fluid is minimized in this configuration, allowing the fluid to flow more freely.
- Thermal distribution increases with an increase in the magnetic factor, radiation factor, Eckert number, exponential heat source, space-based heat source, and decreases with an increase in the inclination angle and thermal slip factor.
- The Nusselt number increases for both types of nanofluids with increases in various emerging factors in the scenarios of thermal slip and no-slip, where the increase in the Nusselt number is maximum for the scenario where there is no thermal slip.
- The higher thermal distribution and heat transfer rate are determined for the lamina-shaped Cu–water and CuO–water nanofluid flows under both slip and no-slip thermal conditions.
- This study aids industrial cooling by optimizing nanofluid-based heat exchangers, improving thermal performance in microchips, turbines, and reactors. In biomedical applications, enhanced heat transfer supports targeted drug delivery, thermal therapies, and precise temperature regulation in medical devices, where nanoparticle shape control enables more efficient and safer thermal management under complex flow conditions.

7 Future research directions

In future work, some other nanoparticle materials like rod, cube, disk, wire, star-shaped, prism, and ellipsoid will be tested to check their impacts on the heat transfer rate. By expanding the range of particle shapes, the study will aim to identify optimal geometries that maximize heat transfer efficiency under varying flow conditions. This will contribute to the development of more efficient nanofluid-based thermal management systems for industrial and technological applications.

Funding information: This study is supported *via* funding from Prince Sattam bin Abdulaziz University project number (PSAU/2025/R/1446).

Author contributions: H.Y. and A.A.: conceptualization and methodology; E.A.A., F.S.A., and A.A.: software and writing – original draft preparation; F.M.A. and E.A.A.: visualization and investigation; F.S.A., F.M.A., and H.Y.: validation, writing – reviewing, and editing. All authors have accepted responsibility for the entire content of this manuscript and approved its submission.

Conflict of interest: The authors state no conflict of interest.

Data availability statement: The datasets generated and/or analyzed during the current study are available from the corresponding author on reasonable request.

References

[1] Choi S, Eastman J. Enhancing thermal conductivity of fluids with nanoparticles; 1995 [cited 2021 Sep 10]. https://www.osti.gov/biblio/196525.

[2] Shah Z, Khan A, Khan W, Alam MK, Islam S, Kumam P, et al. Micropolar gold blood nanofluid flow and radiative heat transfer between permeable channels. Comput Methods Prog Biomed. 2020;186:105197.

[3] Acharya N, Mabood F, Shahzad SA, Badruddin IA. Hydrothermal variations of radiative nanofluid flow by the influence of nanoparticles diameter and nanolayer. Int Commun Heat Mass Transf. 2022;130:105781.

[4] Khan A, Shah Z, Alzahrani E, Islam S. Entropy generation and thermal analysis for rotary motion of hydromagnetic Casson nanofluid past a rotating cylinder with Joule heating effect. Int Commun Heat Mass Transf. 2020;119:104979.

[5] Bhatti MM, Öztop HF, Ellahi R. Study of the magnetized hybrid nanofluid flow through a flat elastic surface with applications in solar energy. Mater (Basel). 2022;15(21):7507.

[6] Hussain SM, Jamshed W, Safdar R, Shahzad F, Mohd Nasir NAA, Ullah I. Chemical reaction and thermal characteristics of Maxwell

nanofluid flow-through solar collector as a potential solar energy cooling application: A modified Buongiorno's model. Energy Env. 2023;34(5):1409–32.
[7] Abbasi A, Farooq W, Tag-ElDin ESM, Khan SU, Khan MI, Guedri K, et al. Heat transport exploration for hybrid nanoparticle (Cu, Fe_3O_4) – Based blood flow via tapered complex wavy curved channel with slip features. Micromachines. 2022;13(9):1415.
[8] Eid MR, Nafe MA. Thermal conductivity variation and heat generation effects on magneto-hybrid nanofluid flow in a porous medium with slip condition. Waves Random Complex Media. 2022;32(3):1103–27.
[9] Lone SA, Alyami MA, Saeed A, Dawar A, Kumam P, Kumam W. MHD micropolar hybrid nanofluid flow over a flat surface subject to mixed convection and thermal radiation. Sci Rep. 2022;12(1):1–14.
[10] Waqas H, Farooq U, Liu D, Abid M, Imran M, Muhammad T. Heat transfer analysis of hybrid nanofluid flow with thermal radiation through a stretching sheet: A comparative study. Int Commun Heat Mass Transf. 2022 Nov;138:106303.
[11] Rehman A, Saeed A, Bilal M. Analytical study of three-dimensional MHD hybrid nanofluid flow along with thermal characteristics and radiative solar energy. Waves Random Complex Media. 2022;35(4):6383–97.
[12] Rauf A, Faisal, Shah NA, Botmart T. Hall current and morphological effects on MHD micropolar non-Newtonian tri-hybrid nanofluid flow between two parallel surfaces. Sci Rep. 2022;12(1):16608.
[13] Upreti H, Joshi N, Pandey AK, Rawat SK. Homogeneous–heterogeneous reactions within magnetic Sisko nanofluid flow through stretching sheet due to convective conditions using Buongiorno's model. J Nanofluids. 2022;11(5):646–56.
[14] Adnan NKM, Mahmood I, Abbas W, Bani-Fwaz MZ, Eldin SM. Numerical heat featuring in Blasius/Sakiadis flow of advanced nanofluid under dissipation and convective heat condition effects. ZAMM-J Appl Math Mech Angew Math Mech. 2024;104(2):e202200622.
[15] Rahman KU, Adnan, Mishra NK, Bani-Fwaz MZ. Thermal study of Darcy–Forchheimer hybrid nanofluid flow inside a permeable channel by VIM: features of heating source and magnetic field. J Therm Anal Calorim. 2023;148(24):14385–403.
[16] Alharbi KAM, Adnan, Bani-Fwaz MZ, Eldin SM, Akgul A. Thermal management in annular fin using ternary nanomaterials influenced by magneto-radiative phenomenon and natural convection. Sci Rep. 2023;13(1):9528.
[17] Bani-Fwaz MZ, Mahmood Z, Bilal M, EI-Zahhar AA, Khan I, Niazai S. Computational investigation of thermal process in radiated nanofluid modulation influenced by nanoparticles (Al_2O_3) and molecular (H_2O) diameters. J Comput Des Eng. 2024;11(2):22–36.
[18] Rawat SK, Negi S, Upreti H, Kumar M. A non-Fourier's and non-Fick's approach to study MHD mixed convective copper water nanofluid flow over flat plate subjected to convective heating and zero wall mass flux condition. Int J Appl Comput Math. 2021;7:1–27.
[19] Upreti H, Bartwal P, Pandey AK, Makinde OD. Heat transfer assessment for Au-blood nanofluid flow in Darcy-Forchheimer porous medium using induced magnetic field and Cattaneo-Christov model. Numer Heat Transf Part B Fundam. 2023;84(4):415–31.
[20] Upreti H, Joshi N, Pandey AK, Rawat SK. Assessment of convective heat transfer in Sisko fluid flow via stretching surface due to viscous dissipation and suction. Nanosci Technol An Int J. 2022;13(2):31–44.
[21] Gangadhar K, Sree TS, Wakif A, Subbarao K. Stefan blowing impact and chemical response of Rivlin–Reiner fluid through rotating convective disk. Pramana. 2024;98(4):1–16.
[22] Ahmed B, Liu D, Nisar Z. Endoscopic analysis of peristaltic propulsion of radiative hydromagnetic nanofluid with lubrication approach and slip constraints. Phys Fluids. 2025;37(2):021917.
[23] Hayat T, Amjad S, Nisar Z, Alsaedi A. Peristalsis of hybrid nanomaterial in convectively heated asymmetric configuration. J Therm Anal Calorim. 2025;150:175–85.
[24] Gangadhar K, Naga Chandrika G, Dinarvand S. Simulation of radiative nonlinear heat dynamism on Buongiorno-modeled nanoliquid through porous inclined plate with adjustable chemical response. Mod Phys Lett B. 2024;38(34):2450347.
[25] Abd-Alla AM, Abo-Dahab SM, Thabet EN, Abdelhafez MA. Impact of inclined magnetic field on peristaltic flow of blood fluid in an inclined asymmetric channel in the presence of heat and mass transfer. Waves Random Complex Media. 2022;35(4):7142–66.
[26] Shah IA, Bilal S, Asjad MI, Tag-ElDin EM. Convective heat and mass transport in Casson fluid flow in curved corrugated cavity with inclined magnetic field. Micromachines. 2022;13(10):1624.
[27] Khan Y, Akram S, Razia A, Hussain A, Alsulaimani HA. Effects of double diffusive convection and inclined magnetic field on the peristaltic flow of fourth grade nanofluids in a non-uniform channel. Nanomaterials. 2022;12(17):3037.
[28] Mohammadi M, Nassab SAG. Combined influences of radiation and inclined magnetic field on natural convection in a cavity with complex geometry. Int Commun Heat Mass Transf. 2022;134:106030.
[29] Hussain S, Zeeshan M. Irreversibility analysis for the natural convection of Casson fluid in an inclined porous cavity under the effects of magnetic field and viscous dissipation. Int J Therm Sci. 2022;179:107699.
[30] Selimefendigil F, Öztop HF. Combined effects of using multiple porous cylinders and inclined magnetic field on the performance of hybrid nanoliquid forced convection. J Magn Magn Mater. 2023;565:170137.
[31] Saeed K, Akram S, Ahmad A, Athar M, Imran M, Muhammad T. Impact of partial slip on double diffusion convection and inclined magnetic field on peristaltic wave of six-constant Jeffreys nanofluid along asymmetric channel. Eur Phys J Plus. 2022;137(3):364.
[32] Gangadhar K, Mary Victoria E, Wakif A. Irreversibility analysis for the EMHD flow of silver and magnesium oxide hybrid nanofluid due to nonlinear thermal radiation. Mod Phys Lett B. 2024;38(33):2450337.
[33] Lone SA, Bossly R, Alduais FS, Al-Bossly A, Khan A, Saeed A. Thermal investigation of magnetized Casson hybrid nanofluid flow through two stretchable angular rotating disks with variable porosity and Cattaneo-Christov heat flux model: a numerical approach. Colloid Polym Sci. 2025;303:529–46.
[34] Gangadhar K, Sujana Sree T, Chamkha AJ. Binary chemical interaction and nonlinearity radiative flux of Williamson fluidic flow through Riga plate. Int J Model Simul. 2024;1–15.
[35] Mahabaleshwar US, Maranna T, Huang HN, Joo SW, Zeidan D. An impact of MHD and radiation on Boussinesq–Stokes suspensions fluid flow past a porous flat plate with mass suction/injection. J Therm Anal Calorim. 2025;150:2517–32.
[36] Gangadhar K, Prameela M, Chamkha AJ, GR B, Kannan T. Evaluation of homogeneous-heterogeneous chemical response on Maxwell-fluid flow through spiraling disks with nonlinear thermal radiation using numerical and regularized machine learning methods. Int J Model Simul. 2024;1–23.

[37] Mahabaleshwar US, Kumar PNV, Nagaraju KR, Bognár G, Nayakar SNR. A new exact solution for the flow of a fluid through porous media for a variety of boundary conditions. Fluids. 2019;4(3):125.
[38] Khan A, Alyami MA, Alghamdi W, Alqarni MM, Yassen MF, Tag Eldin E. Thermal examination for the micropolar gold–blood nanofluid flow through a permeable channel subject to gyrotactic microorganisms. Front Energy Res. 2022;10:993247.
[39] Wehinger D, Eppinger T, Bafakeeh OT, Raghunath K, Ali F, Khalid M, et al. Hall current and Soret effects on unsteady MHD rotating flow of second-grade fluid through porous media under the influences of thermal radiation and chemical. mdpi.com [Internet]; 2022 [cited 2022 Dec 20]. https://www.mdpi.com/2073-4344/12/10/1233.
[40] Zayed ME, Shboul B, Yin H, Zhao J, Zayed AAA. Recent advances in geothermal energy reservoirs modeling: Challenges and potential of thermo-fluid integrated models for reservoir heat extraction and geothermal energy piles design. J Energy Storage. 2023;62:106835.
[41] Nabizadeh A, Abbasi M, Siavashi J, Sharifi M, Movaghar MRK. Fluid flow modeling through pressure-dependent porous media: An analytical solution and a computational fluid dynamics approach. Groundw Sustain Dev. 2022;18:100776.
[42] Habibishandiz M, Saghir MZ. A critical review of heat transfer enhancement methods in the presence of porous media, nanofluids, and microorganisms. Therm Sci Eng Prog. 2022;30:101267.
[43] Verma AK, Bhattacharyya K, Rajput S, Mandal MS, Chamkha AJ, Yadav D. Buoyancy driven non-Newtonian Prandtl-Eyring nanofluid flow in Darcy-Forchheimer porous medium over inclined non-linear expanding sheet with double stratification. Waves Random Complex Media. 2022;35(3):4424–56.
[44] Sharma BK, Kumar A, Gandhi R, Bhatti MM. Exponential space and thermal-dependent heat source effects on electro-magneto-hydrodynamic Jeffrey fluid flow over a vertical stretching surface. Int J Mod Phys B. 2022;36(30):2250220.
[45] Zaydan M, Hamad NH, Wakif A, Dawar A, Sehaqui R. Generalized differential quadrature analysis of electro-magneto-hydrodynamic dissipative flows over a heated Riga plate in the presence of a space-dependent heat source: the case for strong suction effect. Heat Transf. 2022;51(2):2063–78.
[46] Yusuf TA, Kareem RA, Adesanya SO, Gbadeyan JA. Entropy generation on MHD flow of a Casson fluid over a curved stretching surface with exponential space-dependent heat source and nonlinear thermal radiation. Heat Transf. 2022;51(2):2079–98.
[47] Gangadhar K, Mary Victoria E, Chamkha AJ. Hydrothermal features in the swirling flow of radiated graphene–Fe_3O_4 hybrid nanofluids through a rotating cylinder with exponential space-dependent heat generation. Waves Random Complex Media. 2022;1–24.
[48] Mebarek-Oudina F, Dharmaiah G, Balamurugan KS, Ismail AI, Saxena H. The role of quadratic-linearly radiating heat source with Carreau nanofluid and exponential space-dependent past a cone and a wedge: a medical engineering application and renewable energy. J Comput Biophys Chem. 2023;22(8):997–1011.
[49] Farooq U, Waqas H, Khan MI, Khan SU, Chu YM, Kadry S. Thermally radioactive bioconvection flow of Carreau nanofluid with modified Cattaneo-Christov expressions and exponential space-based heat source. Alex Eng J. 2021;60(3):3073–86.
[50] Rana P, Gupta V, Kumar L. Thermal instability analysis in magneto-hybrid nanofluid layer between rough surfaces with variable gravity and space-dependent heat source. Int J Mod Phys B. 2023;38(4):2450051.
[51] Rafique K, Mahmood Z, Khan U. Mathematical analysis of MHD hybrid nanofluid flow with variable viscosity and slip conditions over a stretching surface. Mater Today Commun. 2023;36:106692.
[52] Farooq M, Walie MH, Ahmad S, Hassine SBH. Assessment of squeezing phenomenon in non-linear stratified fluid flow with slip conditions through Darcy porous material. Int Commun Heat Mass Transf. 2023;146:106945.
[53] Ramzan M, Shahmir N, Saleel CA, Kadry S, Eldin SM, Saeed AM. Model-based comparison of hybrid nanofluid Darcy-Forchheimer flow subject to quadratic convection and frictional heating with multiple slip conditions. Numer Heat Transf Part A Appl. 2023;85(18):3013–33.
[54] Al Rashdi SAS, Ghoneim NI, Amer AM, Megahed AM. Investigation of magnetohydrodynamic slip flow for Maxwell nanofluid over a vertical surface with Cattaneo-Christov heat flux in a saturated porous medium. Results Eng. 2023;19:101293.
[55] Nazeer M, Khan MI, Abdullaev S, Awwad FA, Ismail EAA. Rheological study of Hall current and slip boundary conditions on fluid–nanoparticle phases in a convergent channel. Nanoscale Adv. 2023;5(23):6473–88.
[56] Amer AM, Al Rashdi SAS, Ghoneim NI, Megahed AM. Tangent hyperbolic nanofluid flowing over a stretching sheet through a porous medium with the inclusion of magnetohydrodynamic and slip impact. Results Eng. 2023;19:101370.
[57] Rasool G, Xinhua W, Lund LA, Yashkun U, Wakif A, Asghar A. Dual solutions of unsteady flow of copper-alumina/water based hybrid nanofluid with acute magnetic force and slip condition. Heliyon. 2023;9(12):e22737.
[58] Lone SA, Bossly R, Alduais FS, Al-Bossly A, Khan A, Saeed A. Blood based magnetohydrodynamic casson hybrid nanofluid flow on convectively heated bi-directional porous stretching sheet with variable porosity and slip constraints. Chin Phys B. 2024;34(1):014101.
[59] Swain K, Animasaun IL, Ibrahim SM. Influence of exponential space-based heat source and Joule heating on nanofluid flow over an elongating/shrinking sheet with an inclined magnetic field. Int J Ambient Energy. 2022;43(1):4045–57.
[60] Adnan, Ashraf W. Thermal efficiency in hybrid (Al_2O_3-CuO/H_2O) and ternary hybrid nanofluids (Al_2O_3-CuO-Cu/H_2O) by considering the novel effects of imposed magnetic field and convective heat condition. Waves Random Complex Media. 2022;35(4):8029–44.
[61] Kumar Mishra N, Adnan, ur Rahman K, M. Eldin S, Z. Bani-Fwaz M. Investigation of blood flow characteristics saturated by graphene/CuO hybrid nanoparticles under quadratic radiation using VIM: study for expanding/contracting channel. Sci Rep. 2023;13(1):8503.
[62] Dawar A, Thumma T, Islam S, Shah Z. Optimization of response function on hydromagnetic buoyancy-driven rotating flow considering particle diameter and interfacial layer effects: Homotopy and sensitivity analysis. Int Commun Heat Mass Transf. 2023 [cited 2023 Apr 9];144:106770, https://linkinghub.elsevier.com/retrieve/pii/S0735193323001598.
[63] Basit MA, Farooq U, Imran M, Fatima N, Alhushaybari A, Noreen S, et al. Comprehensive investigations of (Au-Ag/Blood and Cu-Fe_3O_4/Blood) hybrid nanofluid over two rotating disks: Numerical and computational approach. Alex Eng J. 2023;72:19–36.
[64] Rashid U, Ibrahim A. Impacts of nanoparticle shape on Al_2O_3-water nanofluid flow and heat transfer over a non-linear radically stretching sheet. Adv Nanopart. 2020;9(1):23–39.
[65] Lin Y, Li B, Zheng L, Chen G. Particle shape and radiation effects on Marangoni boundary layer flow and heat transfer of copper-water

nanofluid driven by an exponential temperature. Powder Technol. 2016;301:379–86.
[66] Hamad MAA. Analytical solution of natural convection flow of a nanofluid over a linearly stretching sheet in the presence of magnetic field. Int Commun Heat Mass Transf. 2011;38(4):487–92.
[67] Wang CY. Free convection on a vertical stretching surface. ZAMM-J Appl Math Mech Angew Math Mech. 1989;69(11):418–20.
[68] Reddy Gorla RS, Sidawi I. Free convection on a vertical stretching surface with suction and blowing. Appl Sci Res. 1994;52(3):247–57.